*applied sciences*

MDPI

*Article*

# Structural Modal Time Domain Identification Method Based on the Bayesian Uncertain Quantification

**Yaozong Pan [1] and Yan Zhao [1,2,*]**

[1] State Key Laboratory of Structural Analysis, Optimization and CAE Software for Industrial Equipment, School of Mechanics and Aerospace Engineering, Dalian University of Technology, Dalian 116023, China; panyaozong@mail.dlut.edu.cn
[2] NingBo Institute, Dalian University of Technology, Ningbo 315016, China
* Correspondence: yzhao@dlut.edu.cn

**Abstract:** Based on the Bayesian framework, a time domain method is proposed for the uncertain quantification of structural modal identification. First, a theoretical prediction model is constructed from the state space model in modal space and then transformed into physical space using the modal basis. Second, taking into account the uncertainty of the identification results caused by measurement noise and modeling errors, the negative log-likelihood function is constructed using time domain measurement data and a theoretical prediction model based on the Bayesian system identification framework. Finally, an unconstrained quadratic function for the identification parameters is derived through matrix vectorization, and, by mathematically transforming the optimization problem, only the dynamic spectral parameters (the natural frequencies and damping ratios) need to be identified, while the spatial parameters (the mode shapes and modal contribution factors) can be analytically calculated from the spectral parameters, which greatly reduces the dimensionality of the identification parameters. In numerical examples, the identification of the modal parameters for a spring–mass system and high-speed pantograph was studied, and the identified modal parameters based on the simulation response's data were in good agreement with the theoretical values. Moreover, the modal parameters of the actual structure of the pantograph were identified based on the experimental data, and the identifying uncertainties were quantified by the coefficient of variation.

**Keywords:** Bayesian approach; modal state space model; uncertainty quantification; experimental modal analysis

check for updates

**Citation:** Pan, Y.; Zhao, Y. Structural Modal Time Domain Identification Method Based on the Bayesian Uncertain Quantification. *Appl. Sci.* **2024**, *14*, 9927. https://doi.org/10.3390/app14219927

Academic Editor: Junhong Park

Received: 1 September 2024
Revised: 23 October 2024
Accepted: 24 October 2024
Published: 30 October 2024

**Copyright:** © 2024 by the authors. Licensee MDPI, Basel, Switzerland. This article is an open access article distributed under the terms and conditions of the Creative Commons Attribution (CC BY) license (https://creativecommons.org/licenses/by/4.0/).

## 1. Introduction

Modal identification involves the determination of structural modal parameters, such as natural frequency, damping ratios, and mode shapes, using structural input and measured response data. It is widely used in structural performance evaluation, structural vibration control, structural fault diagnosis, and health monitoring [1–3].

Modal identification is typically categorized into Experimental Modal Analysis (EMA) and Operational Modal Analysis (OMA), depending on whether the system inputs are known or unknown during the analysis process. OMA takes the environmental excitations (wind, traffic, micro-vibrations, etc.) as the system inputs and models them as a uniform broadband random noise. Since the OMA methods do not require manual intervention, they can be continuously applied throughout the life cycle of the structure, offering significant economic and practical advantages [4,5]. However, the OMA methods also exhibit certain limitations, particularly when the environmental excitation is of low intensity. In such cases, the measured response exhibits a low amplitude and a reduced signal-to-noise ratio, which makes it challenging to accurately determine the damping ratio [6,7]. In addition, for some mechanical structures, the environmental excitations under operating conditions contain harmonic excitation, which can significantly affect the identification

results when the harmonic excitation amplitude is high [8]. EMA uses excitation and response signals for the modal parameter identification, and one of its main advantages is that the loading equipment (impulse hammer, shaking table, etc.) can achieve different types of excitation. It can obtain measurement signals with a high signal-to-noise ratio through controllable experimental conditions, achieving the accurate identification of high-performance equipment modal parameters [9]. Due to limited excitation energy, EMA is more suitable for the modal parameter identification of small- and medium-sized structures; in addition, EMA does not easily simulate the actual working conditions of the structure.

The main idea of EMA frequency domain methods is to obtain the modal parameters by fitting the frequency response function (FRF) of the measured data and the theoretical model, e.g., the weighted least-squares [10], rational fraction polynomial (RFP) [11], and polyreference least-squares complex frequency domain methods (PolyMAX) [12]. When the frequency resolution is low and spectral leakage exists, the identification accuracy of the frequency domain method is not satisfactory. Therefore, scholars have simultaneously carried out research on the time domain identification methods of modal parameters, with the widely used methods including the least-squares complex exponential (LSCE) [13], the polyreference complex exponential (PRCE) [14], the Eigensystem realization algorithm (ERA) [15], and so on. The EMA methods described above only produce point estimates of the modal parameters and do not provide information about their uncertainties. However, many uncertainties need to be taken into account in the process of modal identification, including the limitation of the number of test samples, the errors caused by incomplete modeling of physical phenomena, the measurement noise, etc. These uncertainties lead to statistical uncertainties in the structural dynamic parameters and are of great importance to further develop the EMA method, so that it can take these uncertainties into account.

In statistical inference theory, there are two ways to quantify the identification uncertainty of EMA methods: the "frequency" approach and the Bayesian approach. In "frequency theory", identification uncertainty is defined as the variance of a random variable estimated in repeated experiments. El-kafafy et al. [16,17] obtained the optimal estimates of the modal parameters based on the maximum likelihood estimation algorithm minimizing the error between the measurements and the estimated modal model and quantified the uncertainty through the covariance matrix of the modal parameters. Mellinger et al. [18] gave the covariance matrices of the state space matrices ($\mathbf{A}$, $\mathbf{C}$) and the modal parameters for the input–output subspace approach based on the perturbation method and further derived the covariance of the input matrices ($\mathbf{B}$, $\mathbf{D}$) and the transfer function [19]. In Bayesian system identification methods, probability is used as a measure of the relative plausibility of the identification result given the system model and measurement data, and the goal of modal identification is to determine the posterior probability density function (PDF) of the modal parameters. Au et al. [20] proposed a fast Bayesian identification method for forced vibration tests with a single shaker input and multiple outputs. Ni and Zhang [21,22] further considered the effect of environmental factors on forced vibration modal tests. Ni and Zhang [23,24] also utilized the response under seismic excitation to identify the modal parameters of the structure and quantified the identification uncertainty through a posterior coefficient of variation. Recently, Au [25] developed an uncertainty law for modal parameters with well-separated modes with known single broadband inputs.

All aforementioned Bayesian modal identification methods are performed in the frequency domain and necessitate the application of a Fast Fourier Transform (FFT) to the measured response data. This process introduces additional errors, particularly when the sample size of the measured data is limited. In contrast to the frequency domain approach, the time domain method facilitates the direct utilization of measured response data for modal parameter identification, which minimizes the uncertainty caused by data processing. According to the literature already mastered by the authors, there is currently no relevant work on Bayesian time domain methods for the uncertainty quantification of the structural modal parameter identification based on EMA under deterministic excitation. Assuming that the system input is band-limited Gaussian white noise, Yuen and Katafy-

giotis [26] constructed a multivariate Gaussian probability density function through the autocorrelation function of structural response and established a Bayesian time domain approach for modal updating based on the approximation of a conditional probability expansion of the response. Numerical experiments were conducted on a single degree of freedom system and a four-bay truss to verify the proposed method.

Inspired by the Bayesian FFT method, this paper proposes a Bayesian time domain modal identification uncertainty quantization method based on the modal state space model. This paper is organized as follows. In Section 2, based on the state space model, the functional expressions of modal displacement and acceleration with respect to dynamic spectral parameters are derived in modal space, and a predictive model of the theoretical response in physical space is given through the modal basis. In Section 3, firstly, the negative log-likelihood function (NLLF) is derived according to the Bayesian formula. Secondly, by vectorizing the spatial parameter matrix, a quadratic function involving the spatial parameter vector is derived. Furthermore, an optimization objective function solely focused on spectral parameters is established by applying the function extremum theory, and the spatial parameter can be derived analytically from the spectral parameter. Finally, the posterior covariance matrix of the modal parameters is solved by using the finite difference method. The implementation process of the proposed method is summarized at the end of the subsection. In the numerical example presented in Section 4, the modal identification is carried out using numerical simulation data and experimental data, and the uncertainties in the identified parameters are quantified using the coefficient of variation. A summary of this paper is given in Section 5.

## 2. Time Domain Theoretical Response Prediction Model Based on the Modal State Space Model

Applying the modal coordinate transformations, a linear time-invariant system with orthogonal damping can be represented by a series of decoupled second-order ordinary differential equations with a single degree of freedom (DOF):

$$\ddot{q}_i + 4\pi\zeta_i f_i \dot{q}_i + 4\pi^2 f_i^2 q_i = F_i,\ i = 1, 2, \cdots, m \tag{1}$$

where $f_i$ and $\zeta_i$ are the system's $i$th natural frequency and damping ratio, respectively, which are collectively referred to as the dynamic spectral parameters in this paper, and $F_i$ is the $i$th modal excitation force, which is given by the following:

$$F_i = \gamma_i u \tag{2}$$

where $u$ is the system input in physical space and $\gamma_i$ is the modal contribution factor.

When the system input is a single-point excitation force or the acceleration excitation, $\gamma_i$ can be expressed as follows:

$$\gamma_i = \frac{\boldsymbol{\phi}_i^{\mathrm{T}} \mathbf{B}_o}{\boldsymbol{\phi}_i^{\mathrm{T}} \mathbf{M} \boldsymbol{\phi}_i} \ or\ \gamma_i = -\frac{\boldsymbol{\phi}_i^{\mathrm{T}} \mathbf{M} \mathbf{E}}{\boldsymbol{\phi}_i^{\mathrm{T}} \mathbf{M} \boldsymbol{\phi}_i} \tag{3}$$

where $\boldsymbol{\phi}_i \in R^{n_d \times 1}$ is the $i$th mode shape containing all the DOFs of the structure; $\mathbf{B}_o \in R^{n_d \times 1}$ and $\mathbf{M} \in R^{n_d \times n_d}$ are the input indication matrix and the mass matrix, respectively; and $\mathbf{E} \in R^{n_d}$ is a vector with all elements being 1.

The right term in Equation (1) is related to both $\gamma_i$ and $u$. Dividing both sides of the equation by $\gamma_i$ results in an expression structurally similar to the equation of motion describing a single DOF in physical space:

$$\ddot{\tilde{q}}_i + 4\pi\zeta_i f_i \dot{\tilde{q}}_i + 4\pi^2 f_i^2 \tilde{q}_i = u,\ i = 1, 2, \cdots, m \tag{4}$$

where $\ddot{\tilde{q}}_i = \ddot{q}_i/\gamma_i$, $\dot{\tilde{q}}_i = \dot{q}_i/\gamma_i$, and $\tilde{q}_i = q_i/\gamma_i$ are the modal responses under excitation $u$. $\gamma_i$ is a time-independent constant, and, by comparing equations of motion (4) with (1), it can be seen that the response of the system under the modal excitation $F_i$ can be obtained by scaling up the $\gamma_i$ times after obtaining the responses $\ddot{\tilde{q}}_i$, $\dot{\tilde{q}}_i$, and $\tilde{q}_i$.

The state vector, as follows, can be used to describe the modal displacement and velocity of a structure:

$$\mathbf{v}_i = \begin{Bmatrix} \tilde{q}_i \\ \dot{\tilde{q}}_i \end{Bmatrix} \tag{5}$$

Then, Equation (4) can be expressed in the form of state space:

$$\begin{gathered} \dot{\mathbf{v}}_i = \hat{\mathbf{A}}_i \mathbf{v}_i + \hat{\mathbf{B}} u \\ \hat{\mathbf{A}}_i = \begin{bmatrix} 0 & 1 \\ -4\pi^2 f_i^2 & -4\pi\zeta_i f_i \end{bmatrix}, \ \hat{\mathbf{B}} = \begin{bmatrix} 0 \\ 1 \end{bmatrix} \end{gathered} \tag{6}$$

where $\hat{\mathbf{A}}_i$ is the state transition matrix. For a detailed derivation of Equation (6), please refer to Appendix B.

The measured response is a discrete time series in a structural dynamic test assuming a sampling time interval of $\Delta t$. For a continuous time system represented by Equation (6), the discrete time series are represented by the sampling of continuous time signals:

$$\mathbf{v}_{i,k} = \begin{Bmatrix} \tilde{q}_{i,k} \\ \dot{\tilde{q}}_{i,k} \end{Bmatrix} = \mathbf{v}_i(k\Delta t), \ \ddot{\tilde{q}}_{i,k} = \ddot{\tilde{q}}_i(k\Delta t), \ u_k = u(k\Delta t), \ k = 0, 1, 2, 3, \ldots. \tag{7}$$

Assuming that the system input remains constant within the interval $t \in [k\Delta t, (k+1)\Delta t]$, i.e., $u(t) = u(k\Delta t)$, the equation of motion of the $i$th mode in the discrete time state space form is as follows:

$$\mathbf{v}_{i,k+1} = \mathbf{A}_i \mathbf{v}_{i,k} + \mathbf{B}_i u_k \tag{8}$$

where

$$\mathbf{A}_i = \mathrm{e}^{\hat{\mathbf{A}}_i \Delta t}, \ \mathbf{B}_i = \left(\mathrm{e}^{\hat{\mathbf{A}}_i \Delta t} - \mathbf{I}_2\right)\left(\hat{\mathbf{A}}_i\right)^{-1} \hat{\mathbf{B}} \tag{9}$$

where $\mathbf{I}_2$ is the unit matrix of $2 \times 2$.

Assuming that the initial condition of the system is $\mathbf{v}_{i,0} = 0$, for the sampling time $t = 0, \ \Delta t, \ 2\Delta t, \ \ldots, \ N_s \Delta t$, the input time series of the system is recorded as follows: $u_0, \ u_1, \ u_2, \ \ldots, \ u_{N_s}$. From Equation (8), the state vector of the $i$th mode of the system at the moment $t = k\Delta t$ can be recursively solved as follows:

$$\mathbf{v}_{i,k} = \mathbf{A}_i^{k-1} \mathbf{B}_i u_0 + \mathbf{A}_i^{k-2} \mathbf{B}_i u_1 + \mathbf{A}_i^{k-3} \mathbf{B}_i u_2 + \cdots + \mathbf{B}_i u_{k-1}, \ k = 1, 2, 3, \ldots, N_s \tag{10}$$

From Equation (10), the modal displacement of the system can be given by the following:

$$\tilde{q}_{i,k}(f_i, \zeta_i) = \mathbf{D}_1 \left(\mathbf{A}_i^{k-1} \mathbf{B}_i u_0 + \mathbf{A}_i^{k-2} \mathbf{B}_i u_1 + \mathbf{A}_i^{k-3} \mathbf{B}_i u_2 + \cdots + \mathbf{B}_i u_{k-1}\right) \tag{11}$$

where $\mathbf{D}_1 = \begin{bmatrix} 1 & 0 \end{bmatrix}$.

From Equation (11), it can be seen that through the normalization process applied to Equation (1), the modal response is only a function of the dynamical spectral parameters. This normalization effectively disentangles the dynamical spectral parameters from the modal contribution factor in modal space.

Since the modal displacement, velocity, acceleration, and inputs of the system satisfy the dynamical equilibrium equations at each moment $t = t_k$, according to Equations (4) and (5), one obtains the following:

$$\ddot{\tilde{q}}_{i,k} = u_k - 4\pi^2 f_i^2 \tilde{q}_{i,k} - 4\pi\zeta_i f_i \dot{\tilde{q}}_{i,k} = u_k - \begin{bmatrix} 4\pi^2 f_i^2 & 4\pi\zeta_i f_i \end{bmatrix} \mathbf{v}_{i,k} \tag{12}$$

Substituting Equation (10) into Equation (12), and one then obtains the following:

$$\ddot{\tilde{q}}_{i,k}(f_i,\zeta_i) = u_k - \mathbf{D}_2\left(\mathbf{A}_i^{k-1}\mathbf{B}_i u_0 + \mathbf{A}_i^{k-2}\mathbf{B}_i u_1 + \mathbf{A}_i^{k-3}\mathbf{B}_i u_2 + \cdots + \mathbf{B}_i u_{k-1}\right) \tag{13}$$

where $\mathbf{D}_2 = \begin{bmatrix} 4\pi^2 f_i^2 & 4\pi\zeta_i f_i \end{bmatrix}$.

Up until now, Equations (11) and (13) have established a prediction model of the theoretical modal response. However, the measured signals are described in physical space, and thus the modal responses obtained from Equations (11) and (13) need to be further transformed into physical space.

The modal parameters $\overline{\theta} = \{f_i, \zeta_i, \boldsymbol{\varphi}_i, \gamma_i : i = 1, \ldots, m\}$ are defined. Using $\eta_{i,k}$ to denote modal displacement $q_{i,k}$ or modal acceleration $\ddot{q}_{i,k}$. According to the modal superposition method, the response of the system under the excitation $u_k$ can be given by the following:

$$\mathbf{y}_k(\overline{\theta}) = \sum_{i=1}^{m} \boldsymbol{\varphi}_i \, \eta_{i,k} = \sum_{i=1}^{m} \boldsymbol{\varphi}_i \gamma_i \, \tilde{\eta}_{i,k} \tag{14}$$

where $\boldsymbol{\varphi}_i \in R^n$ is the $i$th mode shape consisting of the measured DOFs.

$\boldsymbol{\psi}_i = \boldsymbol{\varphi}_i \gamma_i$, which will be referred to as the spatial parameters (consisting of the mode shape and modal contribution factor) in this paper, is defined. Constructing the spatial parameter matrix $\overline{\boldsymbol{\psi}} = \begin{Bmatrix} \boldsymbol{\psi}_1 & \boldsymbol{\psi}_2 & \cdots & \boldsymbol{\psi}_m \end{Bmatrix} \in R^{n \times m}$, Equation (14) can be written as follows:

$$\mathbf{y}_k(\overline{\theta}) = \overline{\boldsymbol{\psi}}\tilde{\boldsymbol{\eta}}_k \tag{15}$$

where $\tilde{\boldsymbol{\eta}}_k = \begin{Bmatrix} \tilde{\eta}_{1,k} & \tilde{\eta}_{2,k} & \cdots & \tilde{\eta}_{m,k} \end{Bmatrix}^{\mathrm{T}}$ is the generalized displacement or acceleration vector. Normally, the mode shape to be identified has a norm constraint—$\| \boldsymbol{\varphi}_i \|_2 = 1$—and therefore $\| \boldsymbol{\psi}_i \|_2 = \| \boldsymbol{\varphi}_i \gamma_i \|_2 = \gamma_i$, i.e., $\boldsymbol{\psi}_i$ is no longer norm-constrained.

Finally, Equation (15) establishes a prediction model for the theoretical response of forced vibration based on the modal state space model.

## 3. Bayesian Modal Identification Based on Modal State Space Prediction Models

### *3.1. Time Domain Bayesian Theoretical Framework*

The first step in embedding the theoretical prediction model in Section 2 into the Bayesian identification model is to define the prediction error $\boldsymbol{\epsilon}_k$ such that $\mathbf{y}_k(\overline{\theta}) + \boldsymbol{\epsilon}_k$ is equal to the measurement response $\{\hat{\mathbf{y}}_k \in R^n : k = 1, \ldots, N_s\}$ of the corresponding measured DOF in the actual structure, i.e.,

$$\hat{\mathbf{y}}_k = \mathbf{y}_k(\overline{\theta}) + \boldsymbol{\epsilon}_k \tag{16}$$

Prediction error describes the difference between the theoretical response and the actual measured response, and this paper considers only the uncertainties caused by measurement noise and modeling errors.

Assuming equal variances and stochastic independence for the prediction errors of different measurements of DOFs, $\boldsymbol{\epsilon}_k$ is modeled as the zero mean, which is uncorrelated Gaussian white noise [27]:

$$\boldsymbol{\epsilon}_k \sim N\left(0, \sigma_\epsilon^2 \mathbf{I}_n\right) \tag{17}$$

where $\sigma_\epsilon^2$ is the variance and $\mathbf{I}_n$ is the identity matrix of $n \times n$.

$\theta = \left\{\overline{\theta}, \sigma_\epsilon^2\right\}$ is defined, given the probability model and modeling assumptions. Let $\mathcal{D}$ be the set of measured response data, according to Bayes's theorem, and one obtains the following:

$$p(\theta|\mathcal{D}) = \frac{p(\theta)p(\mathcal{D}|\theta)}{P(\mathcal{D})} \tag{18}$$

where $P(\mathcal{D})$ contains information about the measured response data and is modeled as a normalization constant.

In Bayesian inference, $p(\mathcal{D}|\theta)$ depends entirely on the measured data given parameters $\theta$. It varies faster due to the impact of the data $\mathcal{D}$ compared to $p(\theta)$. Therefore, $p(\mathcal{D}|\theta)$ is the dominant factor for the Bayesian inference. It is usually assumed that $p(\theta)$ follows a uniform distribution [20,24,27], and Equation (18) can be simplified as follows:

$$p(\theta|\mathcal{D}) = \kappa_0 p(\mathcal{D}|\theta) \tag{19}$$

where $\kappa_0$ is a constant containing $P(\mathcal{D})$ and $p(\theta)$.

For the prediction error sequence $\mathcal{D}_\epsilon = \{\epsilon_k \in R^n : k = 1, \ldots, N_s\}$, $\epsilon_k$ is a zero mean Gaussian white noise stochastic process with independent components, and the joint probability density function of $\epsilon_k$ can be given by the probability distribution theory of multivariate random variables [28]:

$$p\left(\mathcal{D}_\epsilon \middle| \sigma_\epsilon^2\right) = \left(2\pi\sigma_\epsilon^2\right)^{-\frac{nN_s}{2}} \exp\left\{-\frac{1}{2\sigma_\epsilon^2}\sum_{k=1}^{N_s}(\epsilon_k)^{\mathrm{T}}\epsilon_k\right\} \tag{20}$$

The likelihood function $p(\mathcal{D}|\theta)$ is obtained by substituting $\epsilon_k = \hat{\mathbf{y}}_k - \mathbf{y}_k(\overline{\theta})$ from Equation (16) into the above equation:

$$p(\mathcal{D}|\theta) = \left(2\pi\sigma_\epsilon^2\right)^{-\frac{nN_s}{2}} \exp\left\{-\frac{1}{2\sigma_\epsilon^2}\sum_{k=1}^{N_s}\left[\hat{\mathbf{y}}_k - \mathbf{y}_k(\overline{\theta})\right]^{\mathrm{T}}\left[\hat{\mathbf{y}}_k - \mathbf{y}_k(\overline{\theta})\right]\right\} \tag{21}$$

Taking the negative logarithm of Equation (21), according to the ln algorithm, the NLLF can be obtained as follows:

$$L(\theta) = -ln(p(\mathcal{D}|\theta)) = \frac{nN_s}{2}\ln(2\pi) + \frac{nN_s}{2}\ln\left(\sigma_\epsilon^2\right) + \frac{1}{2\sigma_\epsilon^2}\sum_{k=1}^{N_s}\left[\hat{\mathbf{y}}_k - \mathbf{y}_k(\overline{\theta})\right]^{\mathrm{T}}\left[\hat{\mathbf{y}}_k - \mathbf{y}_k(\overline{\theta})\right] \tag{22}$$

In the Bayesian approach, the most probable value (MPV) $\theta^*$ maximizes the PDF, and, by the orthogonal relation $p(\theta|\mathcal{D}) \propto e^{-L(\theta)}$, $\theta^*$ minimizes the NLLF, i.e.,

$$\theta^* = \underset{\theta}{\operatorname{argmax}}(p(\theta|\mathcal{D})) = \underset{\theta}{\operatorname{argmin}}(L(\theta)) \tag{23}$$

Therefore, $\theta^*$ can be calculated by solving for the minimum value of $L(\theta)$ with an optimization algorithm.

The MPV in the Bayesian approach is consistent with the results of the maximum likelihood estimation (MLE) in traditional statistical theory due to the assumption that the prior PDF $p(\theta)$ obeys a uniform distribution [29]. However, a distinct advantage of the Bayesian approach is that it can give the posterior covariance matrix of the parameters, thus quantifying the uncertainty of the identification results. When the length of the measured data is large enough, according to Laplace's method of asymptotic approximation, the posterior PDF $p(\mathcal{D}|\theta)$ can be well approximated by a Gaussian PDF [30]:

$$p(\theta|\mathcal{D}) \propto \exp\left[-\frac{1}{2}(\theta - \theta^*)^{\mathrm{T}}(\mathbf{C}^*)^{-1}(\theta - \theta^*)\right] \tag{24}$$

where $\theta^*$ and $\mathbf{C}^*$ are the mean and covariance matrices of parameters $\theta$, respectively. The covariance matrix $\mathbf{C}^*$ is equal to the inverse of the Hessian matrix of the NLLF:

$$\mathbf{C}^* = [\mathbf{H}_L(\theta^*)]^{-1} \tag{25}$$

where $\mathbf{H}_L(\theta^*)$ denotes the Hessian matrix of $L(\theta)$ at $\theta^*$ with elements of $[\mathbf{H}_L(\theta^*)]_{ij} = \frac{\partial^2 L(\theta)}{\partial\theta_i\partial\theta_j}\big|_{\theta=\theta^*}$.

### *3.2. Decoupling Method for Modal Identification*

Let $V$ be the vector space composed of all $2m + mn + 1$ dimensional real vectors, denoted as $\mathbf{R}^{2m+mn+1}$, which satisfies vector addition and multiplication closure. In this paper, the vector $\theta = \begin{bmatrix} f_1 & \cdots & f_m & \zeta_1 & \cdots & \zeta_m & \boldsymbol{\Phi} & \sigma_\epsilon^2 \end{bmatrix}^{\mathrm{T}} \in R^{2m+mn+1}$ is composed of the spectral parameters and mode parameters.

In Equation (22), the following is defined:

$$f(\overline{\theta}) = \sum_{k=1}^{N_s} \left[\hat{\mathbf{y}}_k - \mathbf{y}_k(\overline{\theta})\right]^{\mathrm{T}} \left[\hat{\mathbf{y}}_k - \mathbf{y}_k(\overline{\theta})\right] \tag{26}$$

The first derivative of $L(\theta)$ with respect to $\sigma_\epsilon^2$ is as follows:

$$\frac{\partial L(\theta)}{\partial \sigma_\epsilon^2} = \frac{nN_s}{2\sigma_\epsilon^2} - \frac{f(\overline{\theta})}{2(\sigma_\epsilon^2)^2} \tag{27}$$

Based on the extremum theory of multivariate functions, when the first-order derivative of the likelihood function $L(\theta)$ with respect to the variable $\sigma_\epsilon^2$ is zero, an analytic expression for $\sigma_\epsilon^2$ with respect to $f(\overline{\theta})$ can be derived:

$$\left(\sigma_\epsilon^2\right)^* = \frac{f(\overline{\theta})}{nN_s} \tag{28}$$

and, when $f(\overline{\theta})$ takes the minimum value, $\sigma_\epsilon^2$ also takes the minimum value.

Let $\ell$ denote $f_i$, $\zeta_i$, $\gamma_i$, or $\boldsymbol{\varphi}_i$, and the first derivative of the function $L(\theta)$ with respect to $\ell$ is as follows:

$$\frac{\partial L(\theta)}{\partial \ell} = \frac{1}{2\sigma_\epsilon^2} \frac{\partial f(\overline{\theta})}{\partial \ell} \tag{29}$$

Equation (29) indicates that $\left(\partial f(\overline{\theta})/\partial \ell\right)\big|_{\ell=\ell^*} = 0$ when $\left(\partial L(\theta)/\partial \ell\right)\big|_{\ell=\ell^*} = 0$. Therefore, the MPV of $\overline{\theta}$ needs to be solved for only by minimizing the function $f(\overline{\theta})$.

When minimizing $f(\overline{\theta})$, the dynamic spectral and spatial parameters are coupled if the theoretical prediction model (Equation (15)) is directly substituted into Equation (26). When the number of modes to be identified and measurement channels are large, dozens of unknown parameters are generated, which poses a great challenge for solving the MPV of the parameters using an optimization algorithm. However, subsequent derivations demonstrate that vectorizing the spatial parameter matrix $\overline{\boldsymbol{\psi}}$ alters the mathematical structure of $f(\overline{\theta})$, transforming it into a quadratic function for the unconstrained vector. This allows for the separation of the spatial and spectral parameters by solving for the extremum of the quadratic function. The specific derivation is shown below.

For any matrix $\mathbf{X} \in R^{a\times b}$, the vectorization operator "*vec*" stacks the elements $x_{ij}$ of the matrix $\mathbf{X}$ in columns. Applying the vectorization operator to the spatial parameter matrix $\overline{\boldsymbol{\psi}}$ gives the following:

$$\boldsymbol{\Phi} = vec(\overline{\boldsymbol{\psi}}) = \begin{Bmatrix} \boldsymbol{\psi}_1 \\ \vdots \\ \boldsymbol{\psi}_m \end{Bmatrix} \in R^{nm} \tag{30}$$

According to the algorithm of the vectorization operator, $vec(\mathbf{UDH}) = \left(\mathbf{H}^{\mathrm{T}} \otimes \mathbf{U}\right) vec(\mathbf{D})$, where $\mathbf{U} \in R^{d\times h}$, $\mathbf{D} \in R^{h\times g}$, and $\mathbf{H} \in R^{g\times u}$, and $\otimes$ denotes the Kronecker product. Thus, $\overline{\boldsymbol{\psi}}\widetilde{\boldsymbol{\eta}}_k = vec\left(\overline{\boldsymbol{\psi}}\widetilde{\boldsymbol{\eta}}_k\right) = vec\left(\mathbf{I}_{\mathrm{n}}\overline{\boldsymbol{\psi}}\widetilde{\boldsymbol{\eta}}_k\right)$, and Equation (15) can be rewritten as follows:

$$\mathbf{y}_k(\overline{\theta}) = \overline{\boldsymbol{\psi}}\widetilde{\boldsymbol{\eta}}_k = \left(\widetilde{\boldsymbol{\eta}}_{\mathrm{k}}^{\mathrm{T}} \otimes \mathbf{I}_{\mathrm{n}}\right) \boldsymbol{\Phi} \tag{31}$$

Substituting Equation (31) into Equation (26) and expanding it yields the following functional expression:

$$f\left(\overline{\theta}\right) = \mathbf{\Phi}^{\mathrm{T}}\mathbf{G}\mathbf{\Phi} - 2\mathbf{\Phi}^{\mathrm{T}}\mathbf{R} + \sum_{k=1}^{N_s}\left(\hat{\mathbf{y}}_k^{\mathrm{T}}\hat{\mathbf{y}}_k\right) \tag{32}$$

where

$$\mathbf{G} = \left[\left(\sum_{k=1}^{N_s}\widetilde{\boldsymbol{\eta}}_k\widetilde{\boldsymbol{\eta}}_{\mathrm{k}}^{\mathrm{T}}\right)\otimes\mathbf{I}_n\right] \in R^{nm\times nm}, \mathbf{R} = \sum_{k=1}^{N_s}\left(\widetilde{\boldsymbol{\eta}}_k\otimes\hat{\mathbf{y}}_k\right) \in R^{nm\times 1} \tag{33}$$

For the algorithm of Kronecker product, please refer to Appendix A.

In the real vector space, for a symmetric positive definite matrix $\overline{\mathbf{A}} \in R^{n_r\times n_r}$ and nonzero vectors $\overline{\mathbf{x}} \in R^{n_r}$, $\overline{\mathbf{b}} \in R^{n_r}$, and $c \in R$, a quadratic function $F(\overline{\mathbf{x}}) = \overline{\mathbf{x}}^{\mathrm{T}}\overline{\mathbf{A}}\overline{\mathbf{x}} + 2\overline{\mathbf{b}}^{\mathrm{T}}\overline{\mathbf{x}} + c$ can be constructed [30]. From Equation (32), it can be seen that $f\left(\overline{\theta}\right)$ is a quadratic function with respect to the mode vector $\mathbf{\Phi}$. Since $\mathbf{\Phi}$ is an unconstrained vector, based on the law of derivation of a function with respect to vectors [31], an analytical expression for $\mathbf{\Phi}$ can be derived when the gradient of $f\left(\overline{\theta}\right)$ with respect to the vector $\mathbf{\Phi}$ is zero. The specific derivation is as follows:

$$\frac{\partial f\left(\overline{\theta}\right)}{\partial\mathbf{\Phi}} = 2\left(\mathbf{\Phi}^{\mathrm{T}}\mathbf{G} - \mathbf{R}^{\mathrm{T}}\right) \tag{34}$$

According to $\left(\partial f\left(\overline{\theta}\right)/\partial\mathbf{\Phi}\right)|_{\mathbf{\Phi}=\mathbf{\Phi}^*} = 0$, the analytic solution of the vector $\mathbf{\Phi}^*$ can be given by the following:

$$\mathbf{\Phi}^*(f_i,\zeta_i) = \mathbf{G}^{-1}\mathbf{R} \tag{35}$$

The function $f\left(\overline{\theta}\right)$ has a minimum at $\mathbf{\Phi}^* = \mathbf{G}^{-1}\mathbf{R}$. In Equation (35), since the matrices $\mathbf{G}$ and $\mathbf{R}$ are implicit functions for $f_i$ and $\zeta_i$, $\mathbf{\Phi}^*$ is also a function for $f_i$ and $\zeta_i$.

By evaluating the function $J(\theta)$ at $\mathbf{\Phi}^*$, the optimization objective function $f(f_i,\zeta_i)$ only for $f_i$ and $\zeta_i$ can be given by the following:

$$f(f_i,\zeta_i) = -[\mathbf{R}(f_i,\zeta_i)]^{\mathrm{T}}[\mathbf{G}(f_i,\zeta_i)]^{-1}\mathbf{R}((f_i,\zeta_i)) + \sum_{k=1}^{N_s}\left(\hat{\mathbf{y}}_k^{\mathrm{T}}\hat{\mathbf{y}}_k\right) \tag{36}$$

Equation (36) realizes the decoupling of the dynamic spectral parameters $\{f_i,\zeta_i\}$ and the spatial parameters $\{\boldsymbol{\varphi}_i,\gamma_i\}$. In Equation (32), a total of $2m + nm$ unknown parameters are involved. By contrast, Equation (36) solely incorporates $2m$ unknown parameters, substantially reducing the number of variables to be identified. This transformation significantly improves the computational efficiency of the modal parameter identification.

The MPV of $\{f_i,\zeta_i\}$ can be obtained by searching for $\{f_i,\zeta_i\}$, which minimizes the objective function $f(\{f_i,\zeta_i\})$ through the optimization algorithm, and then $\mathbf{\Phi}^*$ is calculated by Equation (35). The vector $\boldsymbol{\psi}_i^*$ can be extracted from the vector $\mathbf{\Phi}^*$, and the analytical solution of $\gamma_i$ is as follows:

$$\gamma_i^* = \parallel\boldsymbol{\psi}_i^*\parallel_2 \tag{37}$$

The MPV of the mode shape $\boldsymbol{\varphi}_i$ can be given by the following:

$$\boldsymbol{\varphi}_i^* = \frac{\boldsymbol{\psi}_i^*}{\gamma_i^*} \tag{38}$$

Since the mode shape $\boldsymbol{\varphi}_i^*$ is a vector subjected to norm constraint, it is common to express the accuracy of the mode shape identification results by using the 'modal assurance criterion' (MAC), which is defined as the dot product between two mode shape vectors:

$$\text{MAC between}\boldsymbol{\varphi}_i^*\text{and}\hat{\boldsymbol{\varphi}}_i = \frac{\left(\boldsymbol{\varphi}_i^*\right)^{\mathrm{T}}\hat{\boldsymbol{\varphi}}_i}{\left\|\boldsymbol{\varphi}_i^*\right\|_2\left\|\hat{\boldsymbol{\varphi}}_i\right\|_2} \tag{39}$$

where $\hat{\boldsymbol{\varphi}}_i$ is a theoretical result. The closer the value of MAC is to 1, the closer the identified mode shape is to the theoretical result.

### 3.3. Uncertainty Analysis of Modal Parameters

Noise in the measurement data and errors in the theoretical prediction model can introduce uncertainty in the identified modal parameters. Utilizing the given measurements and modeling assumptions, the Bayesian approach estimates the uncertainty of the modal parameters by the posterior variance. From Equation (25), the posterior covariance matrix of the modal parameters is equal to the inverse of the Hessian matrix. Therefore, how to solve the Hessian matrix quickly and accurately is a key issue. For explicit functions, the derivative with respect to the independent variable can be analytically solved; for implicit functions, the finite difference method can be used to calculate the derivative value at the MPV of the parameter.

The second derivative of the NLLF with respect to $\sigma_\epsilon^2$ can be given by the following:

$$\frac{\partial^2 L(\theta)}{\partial (\sigma_\epsilon^2)^2} = \frac{2f(\overline{\theta}) - \sigma_\epsilon^2 n N_s}{2(\sigma_\epsilon^2)^3} \tag{40}$$

Substituting Equation (28) into the above equation yields the following:

$$\left.\frac{\partial^2 L(\theta)}{\partial (\sigma_\epsilon^2)^2}\right|_{\theta=\theta^*} = \frac{nN_s}{2\left[(\sigma_\epsilon^2)^*\right]^2} \tag{41}$$

Let $b$ denote $f_i$, $\zeta_i$, or $\mathbf{\Phi}$. The second derivative of the function $L(\theta)$ with respect to $b$ and $\sigma_\epsilon^2$ is as follows:

$$\frac{\partial^2 L(\theta)}{\partial b \partial (\sigma_\epsilon^2)} = -\frac{1}{2(\sigma_\epsilon^2)^2}\frac{\partial f(\overline{\theta})}{\partial b} \tag{42}$$

Since $\overline{\theta}^*$ makes the function $f(\overline{\theta})$ take an extreme value, i.e., $\left(\partial f(\overline{\theta})/\partial b\right)|_{b=b^*} = 0$, there is the following:

$$\left.\frac{\partial^2 L(\theta)}{\partial b \partial (\sigma_\epsilon^2)}\right|_{\theta=\theta^*} = 0 \tag{43}$$

The second derivative of the NLLF with respect to $b$ can be given by the following:

$$\frac{\partial^2 L(\theta)}{\partial b \partial b} = \frac{1}{2\sigma_\epsilon^2}\frac{\partial^2 f(\overline{\theta})}{\partial b \partial b} \tag{44}$$

Equation (44) needs to be solved for the derivative function of the function $f(\overline{\theta})$ with respect to $f_i$, $\zeta_i$, and $\mathbf{\Phi}$. Let $l_i$ and $l_j$ only denote $f_i$ or $\zeta_i$, $i, j = 1, \ldots, m$. The second derivative function of the function $f(\overline{\theta})$ with respect to $l_i$ and $l_j$ is as follows:

$$\frac{\partial^2 f(\overline{\theta})}{\partial l_i \partial l_j} = \begin{cases} \mathbf{\Phi}^{\mathrm{T}}\left\{\sum\limits_{k=1}^{N_s}\left[\frac{\partial^2 \widetilde{\eta}_{i,k}}{\partial l_i \partial l_i}\left(\mathbf{Q}_i + \mathbf{Q}_i^{\mathrm{T}}\right) + 2\left(\frac{\partial \widetilde{\eta}_{i,k}}{\partial l_i}\right)^2 \mathbf{W}_{ii}\right] \otimes \mathbf{I}_n\right\}\mathbf{\Phi} - 2\psi_i^{\mathrm{T}}\left(\sum\limits_k \frac{\partial^2 \widetilde{\eta}_{i,k}}{\partial l_i \partial l_i}\hat{\mathbf{y}}_k\right), & i = j \\ \mathbf{\Phi}^{\mathrm{T}}\left[\left(\sum\limits_{k=1}^{N_s}\frac{\partial \widetilde{\eta}_{i,k}}{\partial l_i}\frac{\partial \widetilde{\eta}_{j,k}}{\partial l_j}\mathbf{W}_{ij}\right) \otimes \mathbf{I}_n\right]\mathbf{\Phi}, & i \neq j \end{cases} \tag{45}$$

where the $i$th column of the matrix $\mathbf{Q}_i \in R^{m\times m}$ is $\widetilde{\eta}_k$ and the rest of the columns are zero vectors; the $(i,i)$th element of the matrix $\mathbf{W}_{ii} \in R^{m\times m}$ is equal to 1 and the rest of the elements are zero; and the $(i,j)$th and $(j,i)$th elements of the matrix $\mathbf{W}_{ij} \in R^{m\times m}$ are equal to 1 and the rest of the elements are zero.

The second derivative function of the function $f(\overline{\theta})$ with respect to $l_i$ and $\mathbf{\Phi}$ is as follows:

$$\frac{\partial^2 f(\overline{\theta})}{\partial l_i \partial \mathbf{\Phi}} = 2\mathbf{\Phi}^{\mathrm{T}}\left\{\left[\sum_{k=1}^{N_s}\frac{\partial \widetilde{\eta}_{i,k}}{\partial l_i}\left(\mathbf{Q}_{\widetilde{\eta}_k} + \mathbf{Q}_{\widetilde{\eta}_k}^{\mathrm{T}}\right)\right] \otimes \mathbf{I}_n\right\} - 2\sum_{k=1}^{N_s}\left[\frac{\partial \widetilde{\eta}_{i,k}}{\partial l_i}\mathbf{e}_i \otimes \hat{\mathbf{y}}_k^{\mathrm{T}}\right] \tag{46}$$

where $\mathbf{e}_i \in R^m$ is a vector whose $i$th element is equal to one, and the remaining elements are equal to zero.

The second derivative of the function $f(\overline{\theta})$ with respect to $\mathbf{\Phi}$ is a matrix of $mn \times mn$:

$$\frac{\partial^2 f(\overline{\theta})}{\partial \mathbf{\Phi} \partial \mathbf{\Phi}} = 2\left[\left(\sum_{k=1}^{N_s} \underset{\sim}{\eta}_k \underset{\sim}{\eta}_k^{\mathrm{T}}\right) \otimes \mathbf{I}_n\right] \tag{47}$$

Equations (45)–(47) give semi-analytic expressions for the function $f(\overline{\theta})$ with respect to $f_i$, $\zeta_i$, and $\mathbf{\Phi}$, which allows one to solve for the Hessian matrix $\mathbf{H}_f\left(\overline{\theta}^*\right)$. Notice that in Equations (11) and (13), since the modal displacements and accelerations are nonlinear functions for $\{f_i, \zeta_i\}$, it is more difficult to give the analytical expressions of the functions. Therefore, it is necessary to solve for the first and second derivatives of the modal response $\underset{\sim}{\eta}_{i,k}$ with respect to $f_i$ and $\zeta_i$ by the finite difference method for the values of the function at the MPVs of $\{f_i, \zeta_i\}$. The Hessian matrix of $f(\overline{\theta})$ can be written as a chunking matrix as shown below:

$$\mathbf{H}_f\left(\overline{\theta}^*\right) = \begin{bmatrix} \mathbf{H}_{\frac{\partial^2 f(\overline{\theta})}{\partial l_i \partial l_j}}\left(\overline{\theta}^*\right) & \mathbf{H}_{\frac{\partial^2 f(\overline{\theta})}{\partial l_i \partial \mathbf{\Phi}}}\left(\overline{\theta}^*\right) \\ \left[\mathbf{H}_{\frac{\partial^2 f(\overline{\theta})}{\partial l_i \partial \mathbf{\Phi}}}\left(\overline{\theta}^*\right)\right]^{\mathrm{T}} & \mathbf{H}_{\frac{\partial^2 f(\overline{\theta})}{\partial \mathbf{\Phi} \partial \mathbf{\Phi}}}\left(\overline{\theta}^*\right) \end{bmatrix} \tag{48}$$

Finally, the Hessian matrix $\mathbf{H}_L(\theta^*) \in R^{(2m+mn+1)\times(2m+mn+1)}$ can be written as a block diagonal matrix:

$$\mathbf{H}_L(\theta^*) = \begin{bmatrix} \frac{1}{2\left(\sigma_\epsilon^2\right)^*}\mathbf{H}_f\left(\overline{\theta}^*\right) & 0 \\ 0^{\mathrm{T}} & \frac{nN_s}{2\left[\left(\sigma_\epsilon^2\right)^*\right]^2} \end{bmatrix} \tag{49}$$

where $\mathbf{0} \in R^{2m+mn}$ is a zero vector.

The posterior covariance matrix of parameters $\theta$ can be solved from Equation (25). The first $2m$ diagonal elements of $\mathbf{C}^*$ are the posterior variances of $\{f_i, \zeta_i\}$, and the last diagonal element of $\mathbf{C}^*$ is the posterior variance of $\sigma_\epsilon^2$.

For the signal noise, it mainly consists of random noise in the measurement hardware and the quantization error of the digitizer: when the sampling rate is large enough, the quantization error can be ignored; however, random noise is inevitable [30]. In frequency domain identification methods, the effect of random noise can be reduced by averaging multiple FFT results. In the method of this paper, noise reduction can be achieved by combining filtering techniques to avoid false modes caused by random noise. In addition, time domain signals with a high signal-to-noise ratio can be obtained by optimizing excitation methods or using high-sensitivity sensors to improve the reliability of the identification results.

### *3.4. Modal Parameters Identification Algorithm Flow*

Based on the method proposed in this paper, the main flow of identifying the modal parameters is as follows: first, the optimization objective function $f(\{f_i, \zeta_i\})$ is established based on the measured response data; second, the MPVs of the natural frequencies and damping ratios are calculated by minimizing the objective function using the optimization algorithm, and, in turn, analytically solving for the MPVs of the modal contribution factors, mode shapes, and variance of the prediction error; finally, the Hessian matrix is solved using the finite difference method, and the inverse of the Hessian matrix is used to obtain the posterior covariance matrix. This process is illustrated in Figure 1.

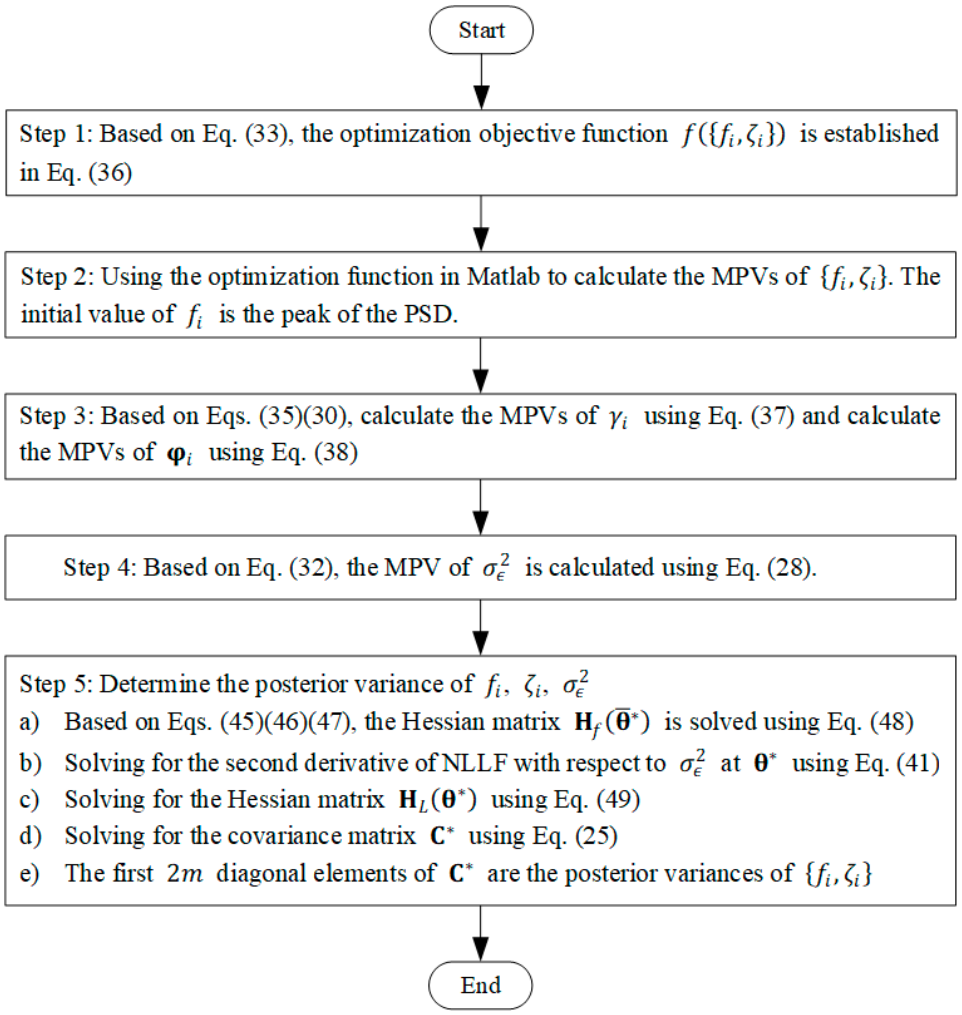



**Figure 1.** Computational flowchart based on the Bayesian time domain identification method.

For the optimization problem in step 2 of Figure 1, the Matlab function "fmincon" was used to find the optimal solution of the spectral parameters that minimizes the objective function. This function can effectively deal with complex multivariate optimization problems and has a high solving efficiency.

## 4. Numerical Examples

### *4.1. Three Degrees of Freedom Spring–Mass System*

This example identifies the modal parameters of the three degrees of freedom system using displacement response signals simulated by the numerical experiments, as shown in Figure 2. The system has linear time-invariant properties and is assumed to have proportional damping. The system stiffness and quality parameters are as follows: $k_1 = 300$ N/m, $k_2 = 50$ N/m, $k_3 = 100$ N/m, $k_4 = 200$ N/m, $m_1 = 0.2$ kg, $m_2 = 0.1$ kg, and $m_3 = 0.3$ kg. The natural frequencies of the system were 3.854, 6.238, and 7.340 Hz, and the damping ratios were all assumed to be 1%. A sinusoidal swept acceleration excitation was applied to the system, and the excitation frequency was linearly increased from 0.1 Hz to 15 Hz within 20 s, with an excitation amplitude of 1 m/s$^2$. The displacement of the three masses was measured with a sampling rate of 100 Hz. The measured responses were simulated by adding independently and identically distributed Gaussian white noise to the theoretical responses.

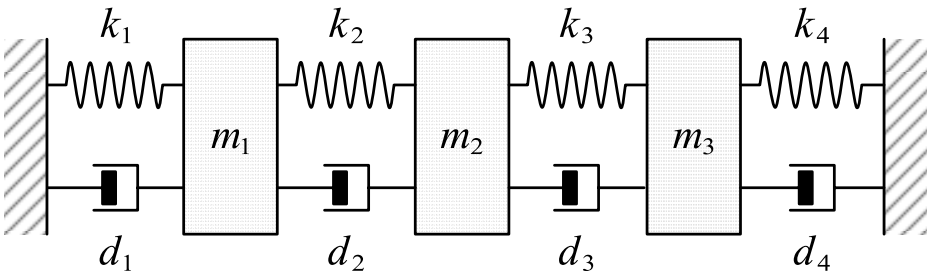



**Figure 2.** Three degrees of freedom spring–mass system.

#### 4.1.1. Nominal Case

The noise level was assumed to be 15%, and the sampling point for each measured channel was 2500. Figure 3 shows the acceleration excitation and displacement response time domain signals of the system. For the optimization solution, the initial values of the natural frequencies were given by the resonance peak of the power spectral density (PSD) of the measured displacement response, and the initial values of the damping ratios were all 0.5%.

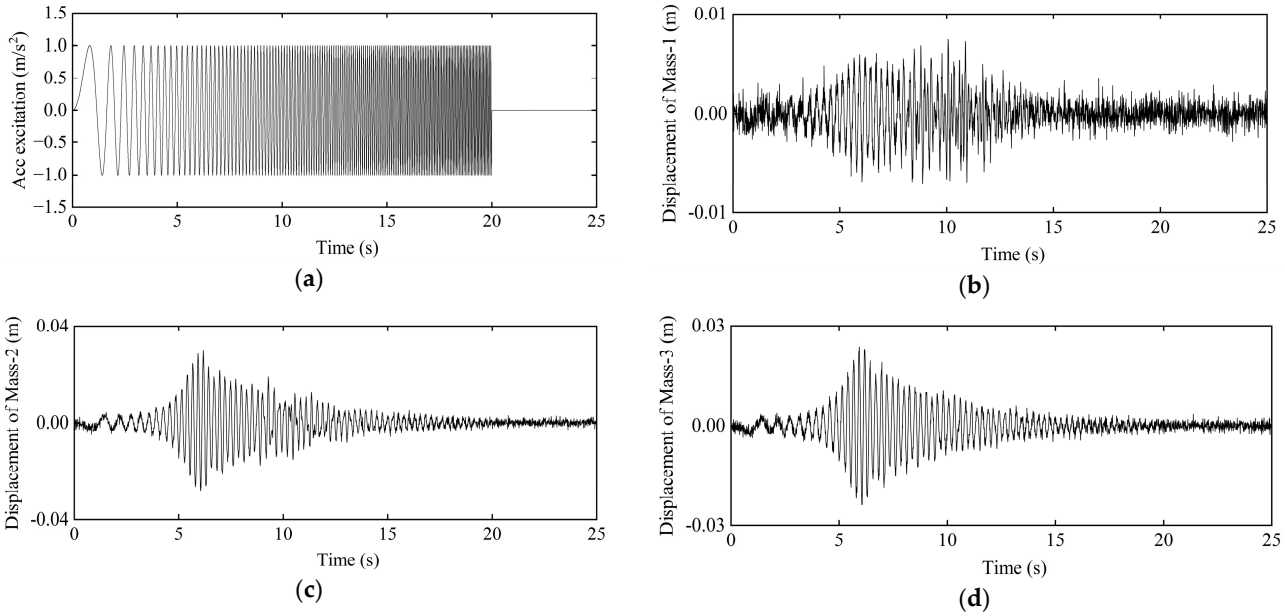



**Figure 3.** Acceleration excitation and measured displacement response of the spring–mass system. (**a**) Sinusoidal swept acceleration excitation; (**b**) Displacement response of mass 1; (**c**) Displacement response of mass 2; (**d**) Displacement response of mass 3.

The results of the modal parameter identification using the proposed method are presented in Table 1. For the natural frequencies, damping ratios, and modal contribution factors, the identification results of the first mode were in perfect agreement with the theoretical values, and the identification results of the remaining two modes had a maximum error of only 4% compared to the theoretical values. The MAC between the identified and theoretical mode shapes was close to 1, indicating that the identified mode shapes were accurate. In addition, the MPV of the variance of the identified prediction error $\sigma_\epsilon^2$ was $8.49 \times 10^{-7}$ and its theoretical value was $8.75 \times 10^{-7}$, with a relative error of only 2.97%.

**Table 1.** Modal identification results and their theoretical values, spring–mass system.

| Parameter | | Mode 1 | Mode 2 | Mode 3 |
|---|---|---|---|---|
| $f$ (Hz) | MPV | 3.854 | 6.237 | 7.338 |
| | Theory | 3.854 | 6.238 | 7.340 |
| $\zeta$ (%) | MPV | 1.00 | 0.96 | 0.96 |
| | Theory | 1.00 | 1.00 | 1.00 |
| $\gamma$ ($10^{-4}$) | MPV | 1.65 | 0.48 | 0.68 |
| | Theory | 1.65 | 0.50 | 0.70 |
| MAC | | 0.9999 | 0.9992 | 0.9990 |

The uncertainties in the identified parameters are listed in Table 2. The posterior uncertainties of the natural frequencies and damping ratios were quantified using the coefficient of variation (COV, COV = posterior standard deviation/MPV). For the natural frequencies, the posterior COVs were very small (<0.03%), whereas the COVs of the damping ratios were above 0.4%, up to 2.869%, indicating that the posterior uncertainties of the natural frequencies were smaller than the damping ratios; this was consistent with typical observations [14,19]. In addition, the COV of the variance of the prediction error $\sigma_\epsilon^2$ was 1.633%.

**Table 2.** Posterior COV of modal parameters, spring–mass system.

| Modal Parameter | Mode 1 | Mode 2 | Mode 3 |
|---|---|---|---|
| $f$ (%) | 0.003 | 0.022 | 0.020 |
| $\zeta$ (%) | 0.464 | 3.190 | 2.869 |

#### 4.1.2. The Effect of Measured Noise

Measured noise can degrade the data quality of the measured response signals, affecting the accuracy of the parameter identification results. Therefore, the effects of different noise levels on the parameter identification results must be discussed. In this subsection, the effect of the measured responses of nine different noise levels on the identification results of the natural frequencies and damping ratios was investigated. The noise levels from low to high levels were as follows: 6, 9, 12, 15, 18, 21, 24, 27, and 30%. The fourth setting is discussed in detail in Section 4.1.1.

Figure 4 shows the identification results of the natural frequencies and damping ratios at different noise levels, where the MPVs of the modal parameters are represented by a dot and the error bar covers ±2 standard deviations. The dashed lines indicate the theoretical values. As shown in the figure, the error bars cover the MPVs of the natural frequencies and damping ratios. With increasing noise levels, the MPVs gradually deviate from the theoretical values, and the extents of the error bars gradually widen (i.e., the standard deviation gradually increases). This observation aligns with our expectation that as the noise level increases, the signal-to-noise ratio of the measured data decreases, leading to greater uncertainties in the identification results.

### *4.2. High-Speed Pantograph Modal*

#### 4.2.1. Numerical Simulation Verification

This section uses the finite element model of a high-speed train pantograph to numerically simulate the actual modal test. The simulation test adopted the hammer excitation method with a single-point excitation and multi-point pickup vibration. Fixed constraints were applied to the base of the pantograph's finite element model, and the pantograph head was a free boundary. The hammering point is shown in Figure 5, and the hammer excitation was simulated using a triangular wave pulse signal with an amplitude of 30 N and a pulse width of 0.01 s. Seven measurement channels were set up on the pantograph head strip to measure the Z-direction's acceleration response, with a sampling frequency of 1000 Hz, a data length of 1500 for each measurement channel, and a measurement

noise level of 20%. The actual measured response was simulated by adding independent identically distributed Gaussian white noise to the theoretical response. All damping ratios were 1%.

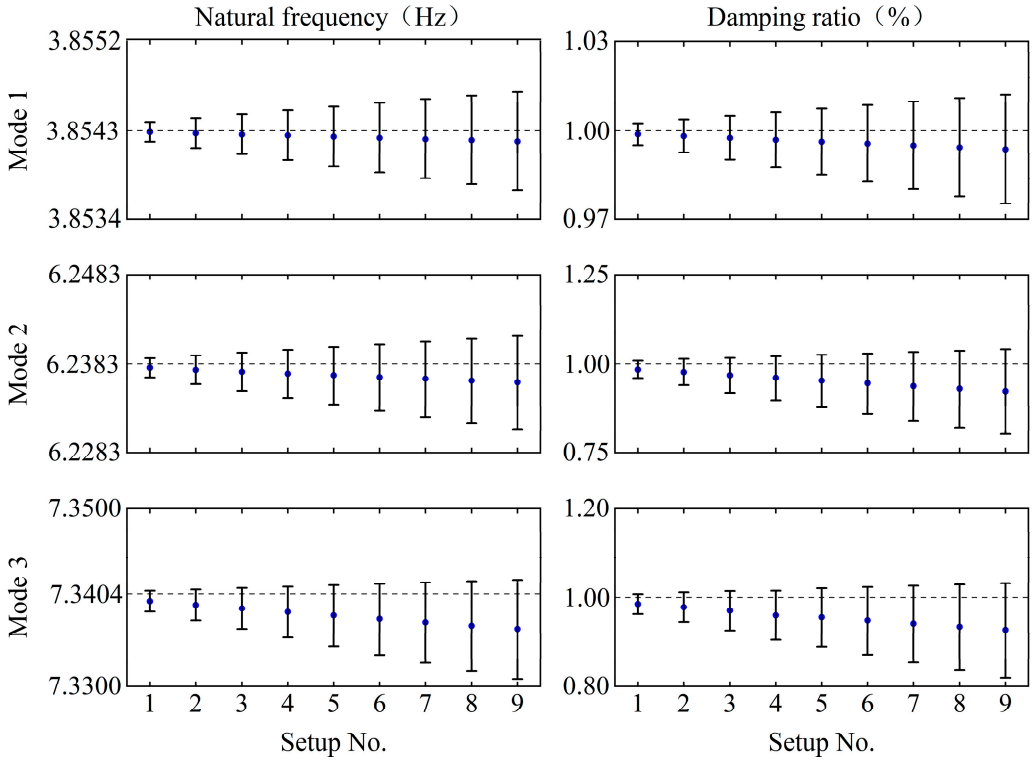



**Figure 4.** Effect of noise level (dot: MPV; and error bar: ±2 standard deviations).

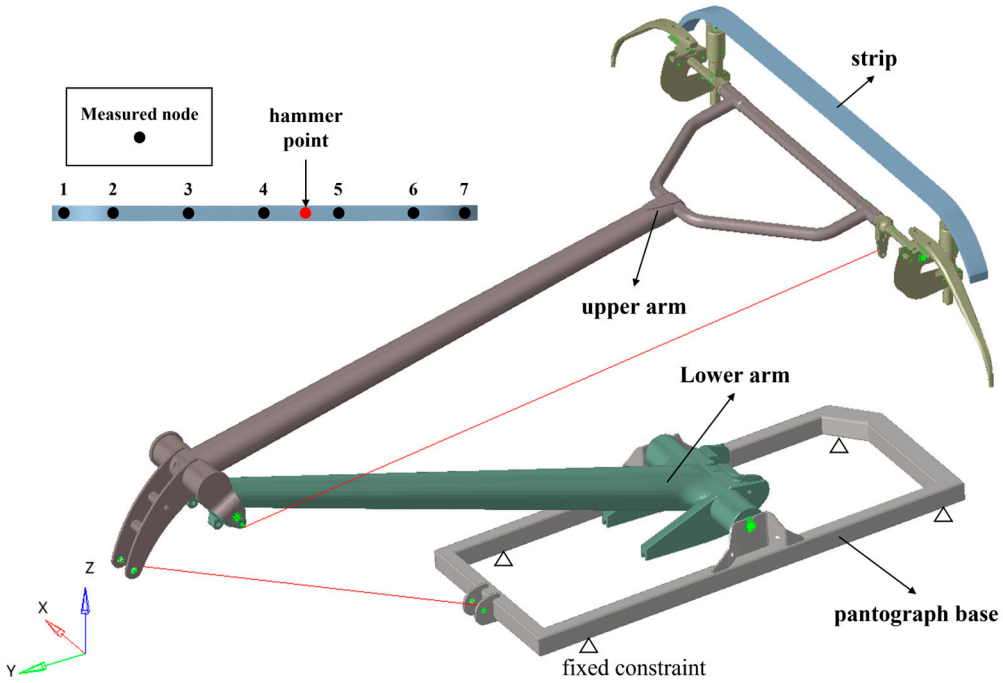



**Figure 5.** Finite element model of pantograph.

The triangular wave pulse excitation force and the acceleration response of measurement node 1 are shown in Figure 6a,b, respectively. The PSD of the acceleration response in the range of 0–140 Hz is shown in Figure 7. Six obvious peaks can be found, including

two pairs of modes with a relatively close natural frequency, i.e., modes 2 and 3 and modes 4 and 5. From the mode shape of the finite element model shown in Figure 8, it can be seen that the mode shapes of the strip in modes 4 and 5 were very similar, with a MAC of 0.96, and modes 4 and 5 were closely spaced. Six modes will be identified simultaneously in the modal identification, which involves solving twelve modal parameters (six natural frequencies and six modal damping ratios) using an optimization algorithm.

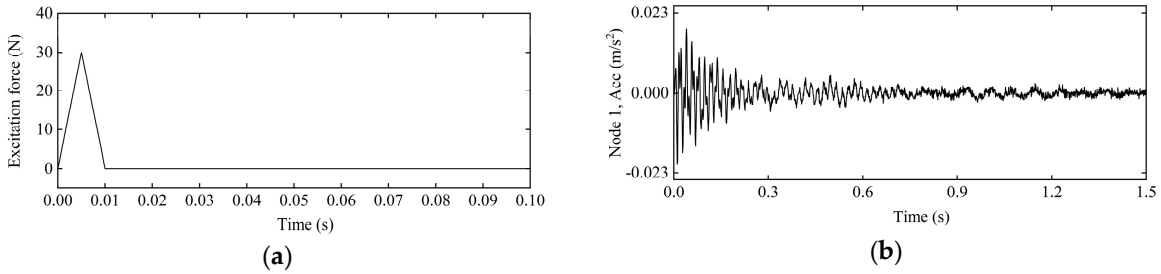



**Figure 6.** Transient excitation and measured acceleration response of pantograph. (**a**) Triangular wave pulse excitation force; (**b**) The acceleration response of measured node 1.

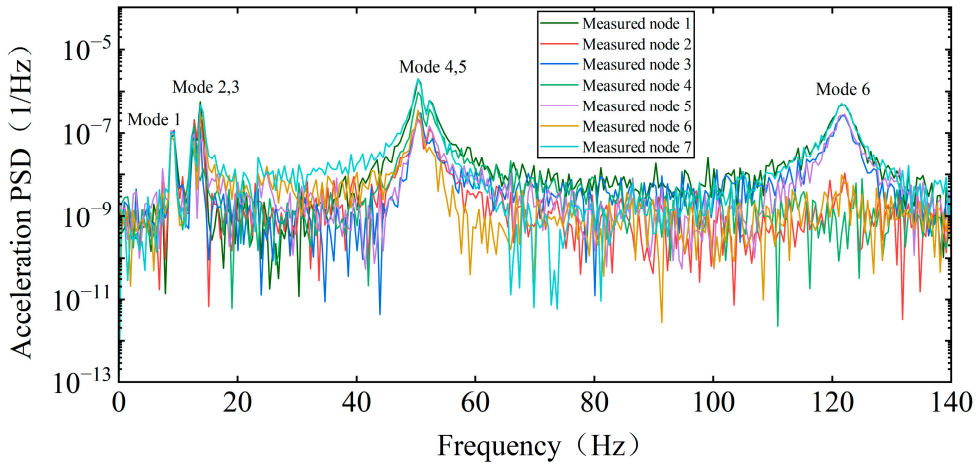



**Figure 7.** PSD of measured acceleration response.

Table 3 shows the modal parameters of the pantograph identified using the method presented in this paper and gives the "theoretical values" of the natural frequencies calculated by the finite element software. For the natural frequencies, the identification results of the first five modes were in good agreement with the "theoretical values", and the maximum error was only 0.21%, while the identification result of the sixth mode was slightly worse compared to the first five, with an error of 1.03%. The identified modal damping ratios were also close to the accurate values, but the accuracy of the damping ratio was more easily affected by the measured noise, which can be verified from the uncertainty analysis results of the damping ratio. Since the MAC between the identified and the finite element mode shape was greater than 0.99, it indicated that the identified mode shape values have a high accuracy. It can also be seen from the results of the mode shape shown in Figure 8 that the identified mode shapes were relatively consistent with the results of the finite element analysis. It can also be seen from the identification results that the method proposed in this paper can also identify close modes. In addition, the MPV of the variance of the identified prediction error $\sigma_\epsilon^2$ was $4.60 \times 10^{-7}$ and its theoretical value was $4.99 \times 10^{-7}$, with a relative error of 7.82%.

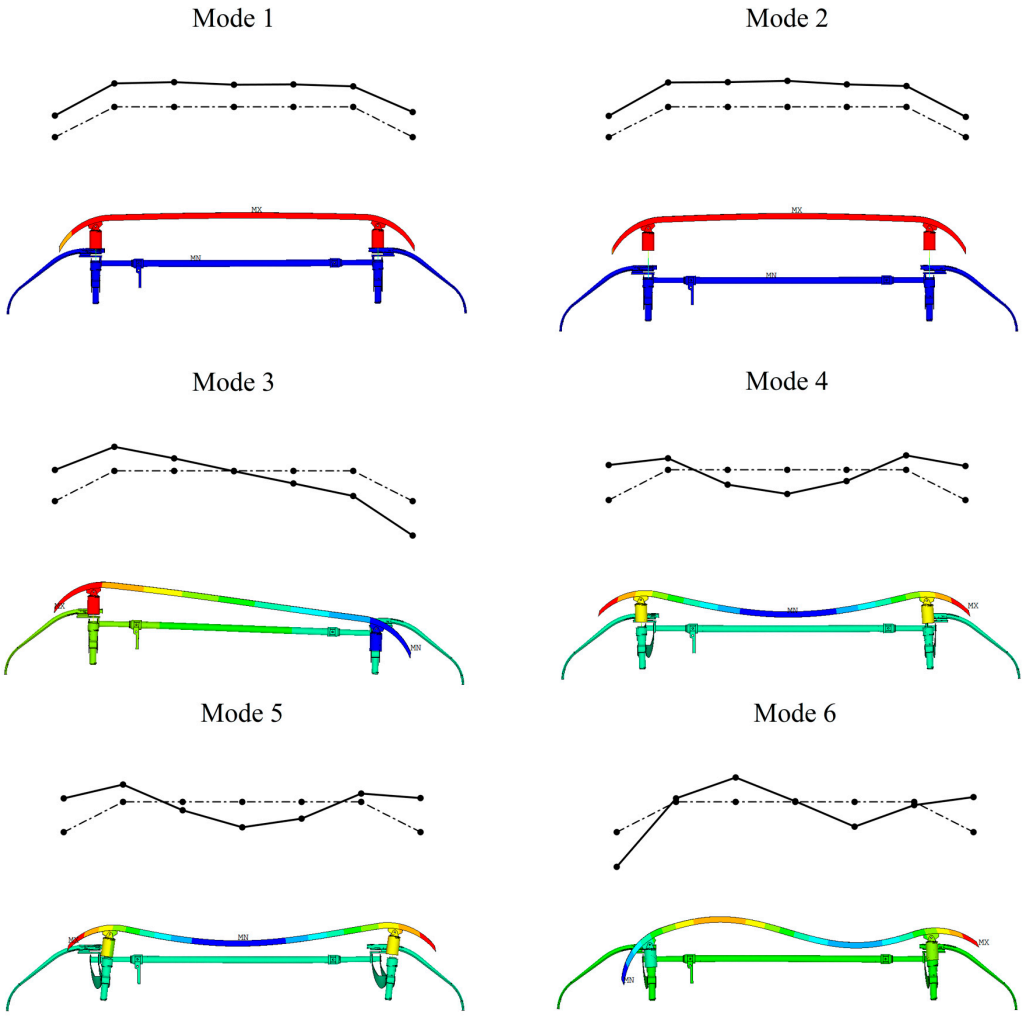



**Figure 8.** Mode shape identification results and finite element analysis results.

**Table 3.** Modal identification results and their theoretical values, pantograph numerical simulation.

| Parameter | | Mode 1 | Mode 2 | Mode 3 | Mode 4 | Mode 5 | Mode 6 |
|---|---|---|---|---|---|---|---|
| $f$ (Hz) | MPV | 9.035 | 12.466 | 13.762 | 50.513 | 52.265 | 122.053 |
| | Theory | 9.035 | 12.472 | 13.764 | 50.585 | 52.376 | 123.320 |
| $\zeta$ (%) | MPV | 1.26 | 1.10 | 1.08 | 0.97 | 1.22 | 1.05 |
| | Theory | 1.00 | 1.00 | 1.00 | 1.00 | 1.00 | 1.00 |
| $\gamma$ ($10^{-4}$) | MPV | 2.4 | 1.7 | 2.4 | 3.3 | 1.9 | 6.1 |
| MAC | | 0.9936 | 0.9975 | 0.9988 | 0.9995 | 0.9984 | 0.9997 |

The posterior COV for the parameters are shown in Table 4. The COVs of natural frequency were less than 0.06%, indicating that the uncertainties of natural frequency were relatively small. However, the COVs of the modal damping ratio were larger than 1% relative to the natural frequency, indicating that measured noise has a greater impact on the identification accuracy of the damping ratio, consistent with the MPVs of the parameters. The COVs were greater than 4% for the first three modes, which were significantly higher than the last three due to the different effects of measured noise on the amplitude of the attenuation response. As shown in Figure 6b, in the initial stage of the acceleration response, the contribution of the last three modes to the response amplitude was greater than that of the first three modes. As the high-frequency response gradually decayed, the response was mainly dominated by the first three modes, which is consistent with the MPVs of the modal contribution factor. Since the Gaussian white noise was applied, the noise intensity was

much smaller than the response amplitude in the initial response stage. With the gradual decay of the response, the actual signal was gradually submerged by the noise. Therefore, the uncertainties of the mode damping ratio of the first three modes were much greater than those of the last three. In addition, the COV of the variance of the prediction error $\sigma_\epsilon^2$ was 1.381%.

**Table 4.** Posterior COV of modal parameters, pantograph numerical simulation.

| Modal Parameter | Mode 1 | Mode 2 | Mode 3 | Mode 4 | Mode 5 | Mode 6 |
|---|---|---|---|---|---|---|
| $f$ (%) | 0.056 | 0.046 | 0.030 | 0.009 | 0.023 | 0.011 |
| $\zeta$ (%) | 7.01 | 6.93 | 4.24 | 1.48 | 3.12 | 1.45 |

In order to further verify the accuracy of the identified results, a transient excitation with an amplitude of 40 N was applied at the same position, and the pulse width remained unchanged. The response of the system under this pulse excitation was predicted using the identified modal parameters and compared with the theoretical response. The results are shown in Figure 9. It can be seen from the figure that the predicted acceleration response and the theoretical acceleration response curve overlap well, indicating that the identified modal parameters are more accurate.

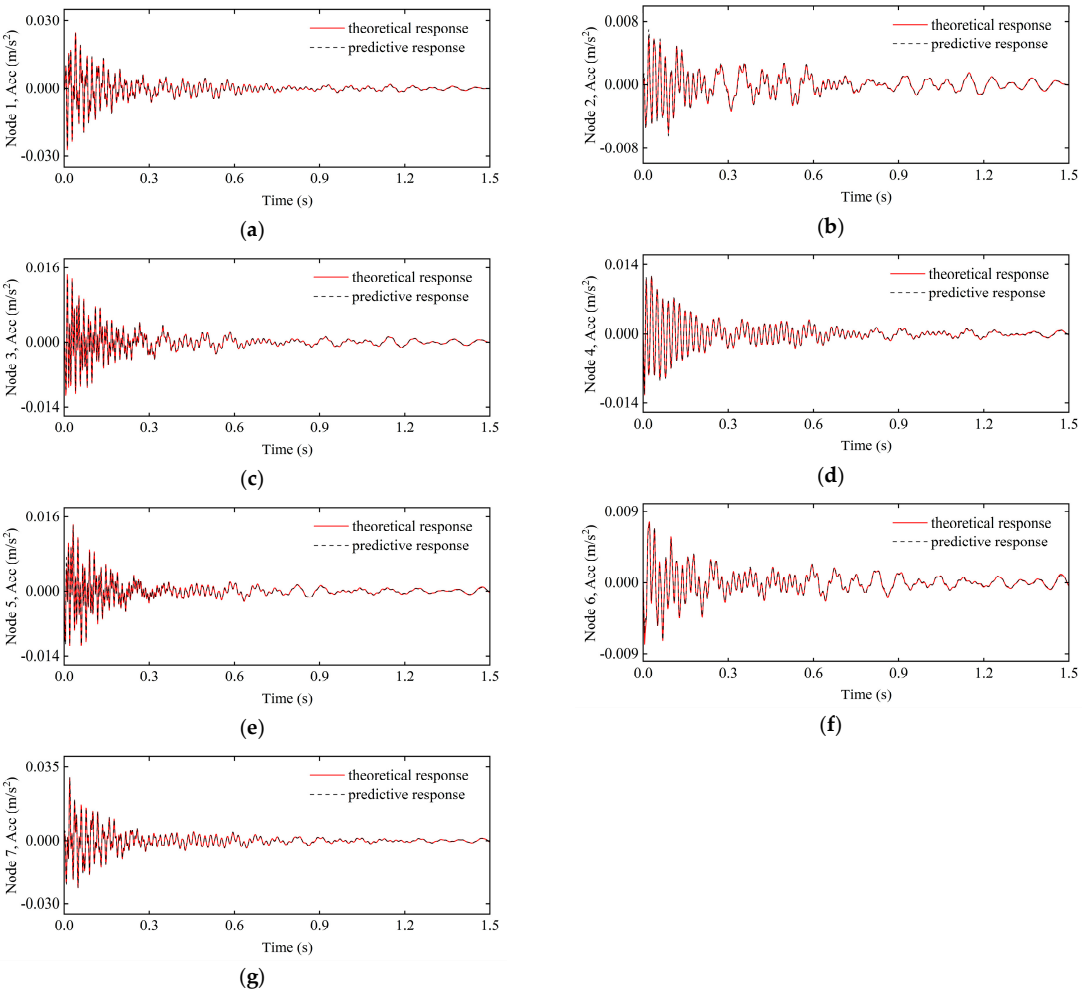



**Figure 9.** Comparison of theoretical and predicted responses of different measured nodes: (**a**) measured node 1, (**b**) measured node 2, (**c**) measured node 3, (**d**) measured node 4, (**e**) measured node 5, (**f**) measured node 6, and (**g**) measured node 7.

#### 4.2.2. Modal Test Verification

In order to verify the effectiveness of the method of this paper in practical tests, the modal parameters of the actual structure of the pantograph were identified using the experimental data in Ref. [32], and the identification results were compared and verified with the deterministic identification results in the literature. Based on the impact load generated by the impulse hammer and the acceleration measurement data of the pickup point, the natural frequencies and damping ratios identified by using the methodology of this paper are shown in Table 5, and the posterior COV of the identified parameters are shown in Table 6.

**Table 5.** Modal identification results and their theoretical values, pantograph modal test.

| Modal Parameter | | Mode 1 | Mode 2 | Mode 3 | Mode 4 | Mode 5 |
|---|---|---|---|---|---|---|
| Proposed methodology | $f$ (Hz) | 10.17 | 12.46 | 49.06 | 134.69 | 221.32 |
| | $\zeta$ (%) | 0.46 | 0.37 | 3.92 | 2.54 | 1.54 |
| Ref. [32] | $f$ (Hz) | 10.0 | 12.5 | 48.4 | 128.5 | 213.0 |

**Table 6.** Posterior COV of modal parameters, pantograph modal test.

| Modal Parameter | Mode 1 | Mode 2 | Mode 3 | Mode 4 | Mode 5 |
|---|---|---|---|---|---|
| $f$ (%) | 0.005 | 0.006 | 0.020 | 0.005 | 0.010 |
| $\zeta$ (%) | 3.845 | 5.141 | 0.699 | 0.347 | 1.054 |

As can be seen from Table 5, the MPVs of the identified natural frequencies exhibit a good agreement with the literature results, and the deviation for the first three modes remains minimal, with the highest relative deviation being 1.36%. Although the deviations for the fourth and fifth modes are slightly larger, with relative deviations of 4.82% and 3.91%, respectively, these deviations remain within an acceptable range of less than 5%. This demonstrates the effectiveness of the proposed method in accurately identifying the modal parameters of the actual structure. The method in this paper also provides the identification results of the damping ratios; however, a comparison of damping ratios is not included in this paper, since only frequency identification was performed in Ref. [32]. In addition, it can be seen from Table 6 that the COV of the damping ratio is much larger than the natural frequency, indicating a greater uncertainty in identifying the damping ratio, which is consistent with the conclusion of the numerical simulation.

## 5. Conclusions

This study presents a Bayesian system identification method that uses the time domain response of a structure. This method applies to cases where a single excitation force or acceleration excitation is used as the system input. In the developed method, the modal bases were used to transform the theoretical predictive model based on the modal state space model into physical space. Addressing the challenge of the coupling between the dynamic spectral parameters and spatial parameters, which complicates the process of finding an optimal solution using optimization algorithms, firstly, the quadratic function for the spatial parameter vector was obtained through the vectorization of the spatial parameter matrix. Then, the optimization objective function for only the spectral parameters was established based on the function extremum, thereby decoupling the spectral and spatial parameters. In addition, in this paper, the posterior covariance matrix of the parameters to be identified was solved by the semi-analytic expression of the derivative function and the finite difference method. The effectiveness of the method was verified using a spring–mass system and a high-speed pantograph model. The identified natural frequencies and damping ratios were extremely close to their theoretical values, and the mode shapes showed the dynamic characteristics of a structure. This method can identify measured

errors consistent with the modeling assumption. Moreover, the proposed method possesses the ability to identify dense modes. The effects of the noise level on the identification results were discussed. As the measurement noise increases, the MPVs of the modal parameters gradually deviate from the theoretical value, and the posterior uncertainties increase.

In addition, the method in this paper can be extended to the modal identification of multi-input linear time-invariant systems. According to the superposition principle, the modal response $\hat{\eta}_l$ of the system under multiple excitations can be obtained by superimposing the modal responses $\hat{\eta}_{l,j}$ under a single excitation ($\hat{\eta}_l = \sum_{j=1}^{N_f} \hat{\eta}_{l,j}$, where $l$ is the number of the modal order and $N_f$ is the number of the system inputs). The physical response $\mathbf{y}_k(\overline{\theta})$ of the system can still be written in the form of the multiplication of the spatial parameter matrix $\hat{\boldsymbol{\psi}}$ with the modal response vector $\hat{\boldsymbol{\eta}}$ ($\mathbf{y}(\overline{\theta}) = \sum_{l=1}^{m} \sum_{j=1}^{N_f} \boldsymbol{\varphi}_l \gamma_{l,j} \hat{\eta}_{l,j} = \hat{\boldsymbol{\psi}} \hat{\boldsymbol{\eta}}$), and then a structural modal identification can be carried out based on the decoupling strategy in Section 3.2.

**Author Contributions:** Conceptualization, Y.P. and Y.Z.; methodology, Y.P. and Y.Z.; software, Y.P.; validation, Y.P.; investigation, Y.P. and Y.Z.; resources, Y.Z.; data curation, Y.P.; writing—original draft preparation, Y.P.; writing—review and editing, Y.Z.; visualization, Y.P.; supervision, Y.Z.; and funding acquisition, Y.Z. All authors have read and agreed to the published version of the manuscript.

**Funding:** This research was funded by the National Natural Science Foundation of China (Nos. 11772084 and U1906233) and the Fundamental Research Funds for the Central Universities (DUT22ZD209 and DUT21ZD209).

**Institutional Review Board Statement:** Not applicable.

**Informed Consent Statement:** Not applicable.

**Data Availability Statement:** The raw data supporting the conclusions of this article will be made available by the authors on request.

**Conflicts of Interest:** The authors declare no conflicts of interest.

## Appendix A

The identity associated with the Kronecker product.

Denote **D**, **J**, **P**, and **W** as matrices with the appropriate dimensions, **a** and **b** as column vectors with the appropriate dimensions, and **I** as a unit matrix with the same dimensions as **b**. The constant equation is useful for the derivation of the formulas in this paper:

$$(\mathbf{D} \otimes \mathbf{J})^{\mathrm{T}} = \mathbf{D}^{\mathrm{T}} \otimes \mathbf{J}^{\mathrm{T}} \tag{A1}$$

$$(\mathbf{D} \otimes \mathbf{J})(\mathbf{P} \otimes \mathbf{W}) = (\mathbf{DP}) \otimes (\mathbf{JW}) \tag{A2}$$

$$(\mathbf{a} \otimes \mathbf{I})\mathbf{b} = \mathbf{a} \otimes \mathbf{b} \tag{A3}$$

## Appendix B

The modal velocity $\dot{\widetilde{q}}_i$ can be rewritten in the following form:

$$\dot{\widetilde{q}}_{ii} = 0 \times \widetilde{q}_i + 1 \times \dot{\widetilde{q}}_i + 0 \times u = \begin{bmatrix} 0 & 1 \end{bmatrix} \begin{bmatrix} \widetilde{q}_i \\ \dot{\widetilde{q}}_i \end{bmatrix} + 0 \times u \tag{A4}$$

From Equation (4), the following can be deduced:

$$\ddot{\widetilde{q}}_i = -4\pi^2 f_i^2 \widetilde{q}_i - 4\pi\zeta_i f_i \dot{\widetilde{q}}_i + u = \begin{bmatrix} -4\pi^2 f_i^2 & -4\pi\zeta_i f_i \end{bmatrix} \begin{bmatrix} \widetilde{q}_i \\ \dot{\widetilde{q}}_i \end{bmatrix} + 1 \times u \tag{A5}$$

Equations (A4) and (A5) can be written together in matrix form, i.e.,

$$\begin{bmatrix} \dot{\tilde{q}}_i \\ \ddot{\tilde{q}}_i \end{bmatrix} = \begin{bmatrix} 0 & 1 \\ -4\pi^2 f_i^2 & -4\pi\zeta_i f_i \end{bmatrix} \begin{bmatrix} \tilde{q}_i \\ \dot{\tilde{q}}_i \end{bmatrix} + \begin{bmatrix} 0 \\ 1 \end{bmatrix} u \tag{A6}$$

where $\mathrm{v}_i = \begin{bmatrix} \tilde{q}_i & \dot{\tilde{q}}_i \end{bmatrix}^{\mathrm{T}}$ is the system state vector and $\dot{\mathrm{v}}_i = \begin{bmatrix} \dot{\tilde{q}}_i & \ddot{\tilde{q}}_i \end{bmatrix}^{\mathrm{T}}$ is the first-order derivative of the state vector with respect to time $t$.

## References


1. Alvin, K.F.; Robertson, A.N.; Reich, G.W.; Park, K.C. Structural system identification: From reality to models. *Comput. Struct.* **2003**, *81*, 1149–1176. [CrossRef]
2. Hamelin, J.L.; Jackson, M.C.; Kirchwey, C.B.; Pileggi, R.A. STS-99 Shuttle Radar Topography Mission Stability and Control. In Proceedings of the AAS/AIAA Conference, Quebec, QC, Canada, 30 July 2001.
3. Reynders, E. System Identification Methods for (Operational) Modal Analysis: Review and Comparison. *Arch. Comput. Method. Eng.* **2012**, *19*, 51–124. [CrossRef]
4. Kim, D.; Kim, M.; Bae, S.G.; Choi, J.W.; Shim, H.B.; Hong, T.; Lee, D.E.; Park, H.S. Field measurements for identification of modal parameters for high-rise buildings under construction or in use. *Autom. Constr.* **2021**, *121*, 103446.
5. Li, J.; Bao, T.; Ventura, C.E. A robust methodology for output-only modal identification of civil engineering structures. *Eng. Struct.* **2022**, *270*, 114764. [CrossRef]
6. Sarlo, R.; Tarazaga, P.A.; Kasarda, M.E. High resolution operational modal analysis on a five-story smart building under wind and human induced excitation. *Eng. Struct.* **2018**, *176*, 279–292. [CrossRef]
7. Bertero, S.; Tarazaga, P.A.; Sarlo, R. In situ seismic testing for experimental modal analysis of civil structures. *Eng. Struct.* **2022**, *270*, 114773. [CrossRef]
8. Jannifar, A.; Zubir, M.N.M.; Kazi, S. An innovative approach for conducting experimental modal analysis (EMA) in running harmonic for structural modal identification. *J. Measurement.* **2020**, *159*, 107795. [CrossRef]
9. Xu, X.; Zhang, H.; Wei, X.; Wu, M.; Zhang, Z. Experimental Study on Natural Vibration Characteristics of Double-Strip High-Speed Pantograph Head. *Exp. Mech.* **2023**, *63*, 995–1001. [CrossRef]
10. Seybert, A. Estimation of damping from response spectra. *Sound Vibr.* **1981**, *75*, 199–206. [CrossRef]
11. Richardson, M.H.; Formenti, D.L. Global Curve Fitting of Frequency Response Measurements using the Rational Fraction Polynomial Method. In Proceedings of the 3rd IMAC, Orlando, FL, USA, 28 January 1985.
12. Peeters, B.; Van der Auweraer, H.; Guillaume, P.; Leuridan, J. The PolyMAX frequency-domain method: A new standard for modal parameter estimation? *Shock Vib.* **2004**, *11*, 395–409. [CrossRef]
13. Brown, D.L.; Allemang, R.J.; Zimmerman, R.; Mergeay, M. Parameter estimation techniques for modal analysis. *SAE Trans.* **1979**, *88*, 828–846.
14. Vold, H.; Kundrat, J.; Rocklin, G.T.; Russell, R. A multi-input modal estimation algorithm for mini-computers. *SAE Trans.* **1982**, *91*, 815–821.
15. Juang, J.N.; Pappa, R.S. An eigensystem realization algorithm for modal parameter identification and model reduction. *J. Guid. Control Dyn.* **1985**, *8*, 620–627. [CrossRef]
16. El-Kafafy, M.; De Troyer, T.; Guillaume, P. Fast maximum-likelihood identification of modal parameters with uncertainty intervals: A modal model formulation with enhanced residual term. *Mech. Syst. Signal Proc.* **2014**, *48*, 49–66. [CrossRef]
17. El-kafafy, M.; De Troyer, T.; Peeters, B.; Guillaume, P. Fast maximum-likelihood identification of modal parameters with uncertainty intervals: A modal model-based formulation. *Mech. Syst. Signal Proc.* **2013**, *37*, 422–439. [CrossRef]
18. Mellinger, P.; Döhler, M.; Mevel, L. Variance estimation of modal parameters from output-only and input/output subspace-based system identification. *J. Sound Vibr.* **2016**, *379*, 1–27. [CrossRef]
19. Greś, S.; Döhler, M.; Jacobsen, N.-J.; Mevel, L. Uncertainty quantification of input matrices and transfer function in input/output subspace system identification. *Mech. Syst. Signal Proc.* **2022**, *167*, 108581. [CrossRef]
20. Au, S.K.; Ni, Y.C. Fast Bayesian modal identification of structures using known single-input forced vibration data. *Struct. Control. Health Monit.* **2014**, *21*, 381–402. [CrossRef]
21. Ni, Y.C.; Zhang, F.L. Fast Bayesian approach for modal identification using forced vibration data considering the ambient effect. *Mech. Syst. Signal Proc.* **2018**, *105*, 113–128. [CrossRef]
22. Ni, Y.-C.; Zhang, F.L. Uncertainty quantification in fast Bayesian modal identification using forced vibration data considering the ambient effect. *Mech. Syst. Signal Proc.* **2021**, *148*, 107078. [CrossRef]
23. Ni, Y.C.; Zhang, F.L. Fast Bayesian frequency domain modal identification from seismic response data. *Comput. Struct.* **2019**, *212*, 225–235. [CrossRef]
24. Ni, Y.C.; Lam, H.F.; Zhang, F.L. Assessing uncertainty in fast Bayesian modal identification based on seismic structural responses. *Mech. Syst. Signal Proc.* **2023**, *185*, 109686. [CrossRef]

25. Ng, C.T.; Wang, P.; Au, S.K.; Li, B. Uncertainty laws of experimental modal analysis with known broadband input. *Mech. Syst. Signal Proc.* **2023**, *204*, 110624. [CrossRef]
26. Yuen, K.V.; Katafygiotis, L.S. Bayesian time–domain approach for modal updating using ambient data. *Probab. Eng. Mech.* **2001**, *16*, 219–231. [CrossRef]
27. Yang, J.H.; Lam, H.F. An innovative Bayesian system identification method using autoregressive model. *Mech. Syst. Signal Proc.* **2019**, *133*, 106289. [CrossRef]
28. Yuen, K.V. *Bayesian Methods for Structural Dynamics and Civil Engineering*; John Wiley & Sons: Hoboken, NJ, USA, 2010.
29. Beck, J.L.; Katafygiotis, L.S. Updating models and their uncertainties. I: Bayesian statistical framework. *J. Eng. Mech.* **1998**, *124*, 455–462. [CrossRef]
30. Au, S.K. *Operational Modal Analysis: Modeling, Bayesian Inference, Uncertainty Laws*; Springer: Berlin, Germany, 2017.
31. Magnus, J.R.; Neudecker, H. *Matrix Differential Calculus with Applications in Statistics and Econometrics*, 3rd ed.; John Wiley & Sons: New York, NY, USA, 2019.
32. Xianghong, X.; Yi, L.; Haochen, Z.; Rui, Z.; Mengzhen, W.; Sijun, H. Full flexible model updating of single-strip pantograph based on modal test. *Chin. J. Theor. Appl. Mech.* **2023**, *55*, 1753–1760.


**Disclaimer/Publisher's Note:** The statements, opinions and data contained in all publications are solely those of the individual author(s) and contributor(s) and not of MDPI and/or the editor(s). MDPI and/or the editor(s) disclaim responsibility for any injury to people or property resulting from any ideas, methods, instructions or products referred to in the content.